Fe-Mn基合金における相平衡と相変態

石 田 清 仁*

*石田清仁 客員フェロー

Phase Equilibria and Phase Transformations in Fe-Mn Based Alloys

Kiyohito ISHIDA*

The α/γ phase equilibria in Fe-Mn based alloys are shown. The large temperature dependence of a change in the partial molar Gibbs energy accompanied by transfer of one mole of Mn from a dilute solution of ferrite to austenite results in a peculiar γ-loop of the Fe-Mn-X (X: ferrite stabilizing element) system due to the magnetic effect. This characteristic feature of α/γ phase equilibria is the origin of the unique martensitic transformation from the bcc parent to the fcc martensite in the Fe-Mn-Al system. A thermodynamic database on the Fe-Mn based alloys, including the elements of C, Al, Si and Cr, by the CALPHAD approach was developed. The design of alloys with high strength and low density using the database is shown. The stacking fault energy of Fe-Mn based alloys is also discussed.

1. INTRODUCTION

The allotropic transformation of iron shows that three crystal structures exist, i.e. α (bcc : ferrite), γ (fcc : austenite), δ (bcc : delta ferrite) and ε (cph), as shown in **Fig. 1** of the P-T (Pressure-Temperature) diagram of iron. The existence of β-Fe has long been recognized, as shown in **Fig. 2**, which shows the Fe-C binary phase diagram by Ledebur's handbook of steel published more than 100 years ago[1]. It is known that β-Fe is the same as α ferrite with bcc structure in the paramagnetic state and is not used at present. Although β-Fe is an old designation, the transformation from α-Fe to β-Fe, that is, magnetic transition, plays a key role in the phase stability of iron, as pointed out by Zener[2]. A typical example of this magnetic effect is shown in **Fig. 3**, where the Fe-C binary phase diagram without consideration of the magnetic contribution in Gibbs energy is presented. If α-Fe is not ferromagnetic, ε-Fe is stable at room temperature, where the ε/γ transition temperature is estimated to be 247°C from extrapolation of the γ/ε phase boundary in the P-T diagram of Fig. 1.

Manganese is known as an austenite stabilizing element but the degree of stability strongly depends on temperature due to the magnetic effect. In this paper, the phase equilibria and phase transformations between α and γ phases in Fe-Mn based alloys are presented. The thermodynamic database constructed by the CALPHAD approach is also shown, and the design of alloys with high strength and low density is reported.

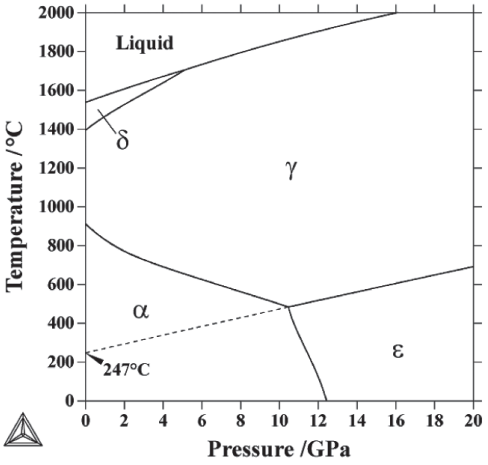

Fig. 1. Pressure-temperature diagram of iron.

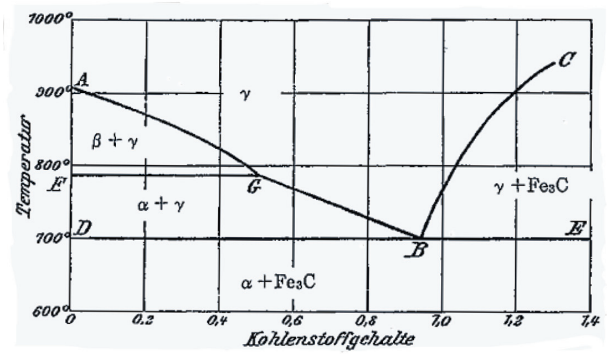

Fig. 2. Fe-C phase diagram in Handbuch der Eisenhuettenkunde by A. Ledebur in 1906.

2017年1月31日 受理

*豊田理化学研究所客員フェロー
東北大学名誉教授，工学博士
専門分野：材料工学，合金設計，組織制御

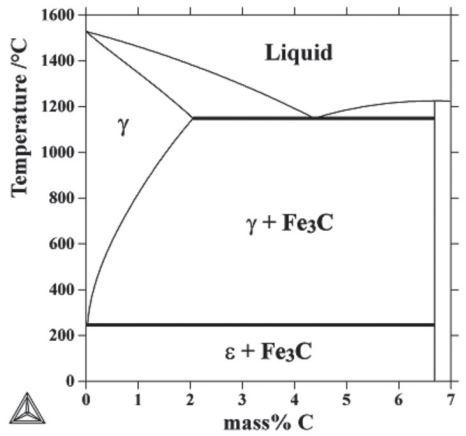

Fig. 3. Calculated Fe-C phase diagram neglecting magnetic contribution of αFe.

2. α/γ EQUILIBRIA of the Fe-Mn-X SYSTEM

The α/γ equilibrium in iron alloys can be classified into two types. One is a γ-loop forming element which stabilizes the ferrite and the other is an expanded γ-field diagram by alloying the austenite stabilizing elements. The parameter $\Delta G_x^{\alpha/\gamma Fe}$, which represents the relative stability of alloying elements between α and γ, is expressed as[3–6)]

$$\Delta G_x^{\alpha/\gamma Fe} = RT \ln \chi_x^{\alpha} / \chi_x^{\gamma} \quad (1)$$

where χ_x^{α} and χ_x^{γ} are the equilibrium compositions of ferrite and austenite at T K, respectively. In dilute solution, eq. (1) can be expressed by regular solution approximation[5,6)],

$$\Delta G_x^{\alpha/\gamma Fe} \approx \Delta G_x^{\alpha\to\gamma} + \Delta\Omega_{Fex}^{\alpha\to\gamma} \quad (2)$$

where $\Delta G_x^{\alpha\to\gamma}$ is the difference in molar Gibbs energy of X between bcc and fcc structure and $\Delta\Omega_{Fex}^{\alpha\to\gamma}$ is the difference in the interaction parameter between the α and γ phases. $\Delta G_x^{\alpha/\gamma Fe}$ is a change in partial molar Gibbs energy accompanied by transfer of one mole of each alloying element from a dilute solution of ferrite to austenite[5,6)]. A schematic illustration of

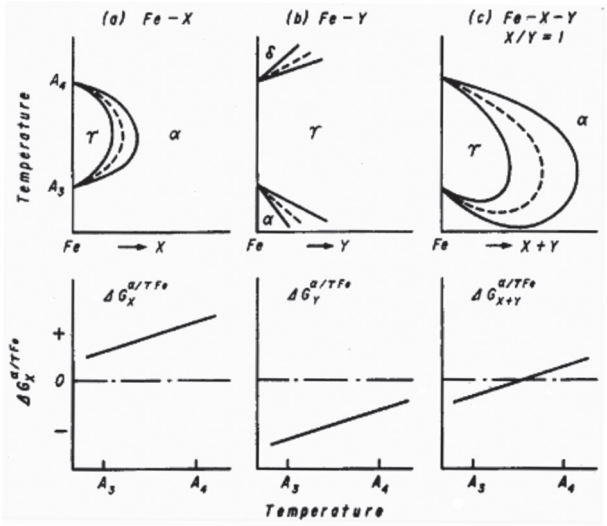

Fig. 4. Schematic illustration of α/γ equilibrium vs $\Delta G_x^{\alpha/\gamma Fe}$ in Fe-X, Fe-Y and Fe-X-Y systems.

α/γ equilibrium for Fe-X, Fe-Y and Fe-X-Y systems is shown in **Fig. 4,** where X and Y are the ferrite and austenite stabilizing elements, respectively and the temperature dependence of $\Delta G_x^{\alpha/\gamma Fe}$ and $\Delta G_y^{\alpha/\gamma Fe}$ is also shown[7)]. If the sign of $\Delta G_{x+y}^{\alpha/\gamma Fe}$ changes from positive to negative value with decreasing temperature, the α/γ equilibrium of Fe-X-Y system shows a peculiar γ-loop similar in shape to that of the Fe-Cr system, where Cr stabilizes ferrite near A_4 temperature while it acts as an austenite stabilizing element near the A_3 temperature. Since $\Delta G_{Mn}^{\alpha/\gamma Fe}$ has a large temperature dependence due to the magnetic effect[6,7)], it is expected that the α/γ equilibria of Fe-Mn-X (X: ferrite stabilizing element) show a γ-loop similar to that shown in Fig. 4(c), which was confirmed experimentally in the Fe-Mn-V, Fe-Mn-Mo and Fe-Mn-Si systems[7)]. Taking account of $\Delta G_x^{\alpha/\gamma Fe}$ for various alloying element, the α/γ equilibria of Fe-Mn-X ternary system at the section of $x_{Mn}/x_{\chi} = 1$ can be classified into seven types[7)], as shown in **Fig. 5**.

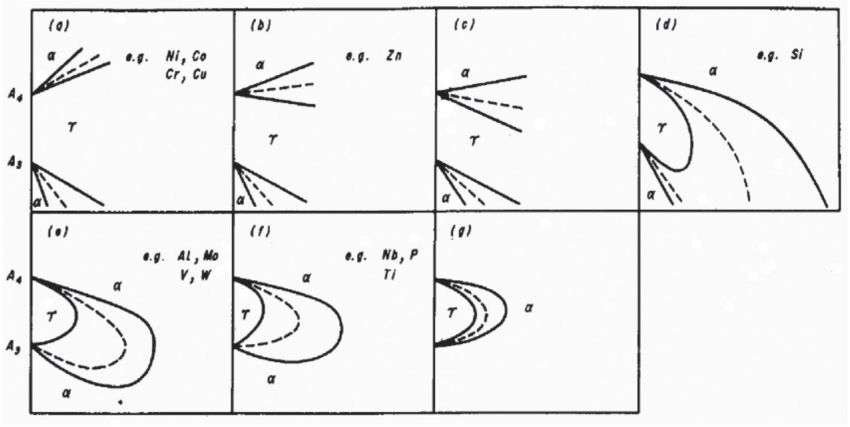

Fig. 5. Classification of γ-loop in Fe-Mn-X systems at $\chi_{Mn}/\chi_x = 1$. Dotted lines represent the *To* lines.
(a) $\Delta G_x^{\alpha/\gamma Fe} < 1046$ (J/mol), (b) $1046 < \Delta G_x^{\alpha/\gamma Fe} < 1130$, (c) $1130 < \Delta G_x^{\alpha/\gamma Fe} < 1234$, (d) $1234 < \Delta G_x^{\alpha/\gamma Fe} < 3264$, (e) $3264 < \Delta G_x^{\alpha/\gamma Fe} < 4916$, (f) $4916 < \Delta G_x^{\alpha/\gamma Fe} < 10293$, (g) $10293 < \Delta G_x^{\alpha/\gamma Fe}$.

3. MARTENSITIC TRANSFORMATION IN Fe-Mn-Al SYSTEM

The peculiar γ-loop of the Fe-Mn-X system as shown in Fig. 5(d) results in unique martensitic transformation (MT). **Figure 6** shows the same shape of γ-loop as that in Fig. 5(d), where two *To* lines and *Ms* temperatures are drawn. At a lower concentration of Mn+X, conventional MT from γ to α' occurs and $Ms^{\gamma\to\alpha'}$ is located below the $To^{\alpha/\gamma}$ temperature where the Gibbs energies of the α and that of the γ phase are equal, while at higher compositions, the $Ms^{\alpha\to\gamma'}$ temperature of α to γ' transformation exists below another $To^{\alpha/\gamma}$ line[8]. This situation is the origin of the occurrence of MT from the α to γ' phase in the Fe-Mn-Al[8] and Fe-Mn-Ga[9] systems. **Figure 7** shows the calculated *To* line for Fe-(20~40) Mn-Al (at %) alloys based on the thermodynamic assessment[10, 11]. The dotted line shows the Curie temperatures of the α phase estimated from the experimental data. The *To* lines for Fe-(20~30) Mn-Al curve to lower Al content near the Curie temperature, which means that the conventional $\gamma\to\alpha'$ MT would occur, while those for Fe-(36~40)Mn-Al suggest $\alpha\to\gamma'$ MT. **Figure 8** shows the optical micrograph of $\alpha\to\gamma'$ MT in the Fe-36Mn-15Al alloy. The martensite remains even at 500°C on heating, which shows the non-thermoelastic MT. **Figure 9** shows the X-ray diffraction patterns taken from the Fe-36Mn-15Al alloy sheets (a) as — quenched and (b) cold-rolled to a reduction rate of 50%, respectively. It is seen that while the fcc martensite indexed as the γ' phase coexists with the α bcc parent (P) phase in the as-quenched state, as shown in Fig. 9(a), the peaks from the α phase disappear in the cold-rolled specimen and the γ' martensite is perfectly induced by deformation to 50% reduction (Fig. 9(b)).

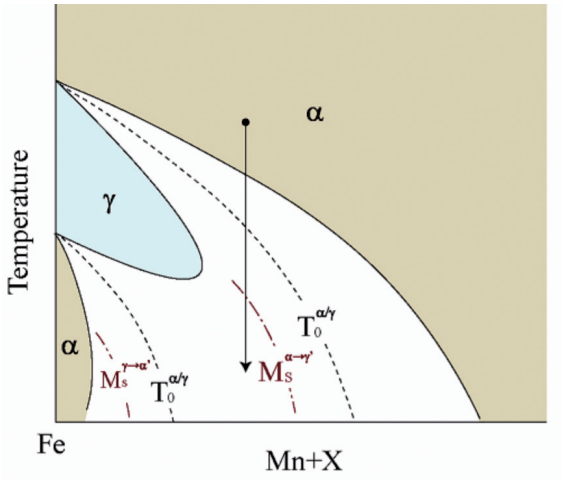

Fig. 6. Schematic illustration of α/γ phase equilibrium related to $To^{\alpha/\gamma}$ and *Ms* temperatures in Fe-Mn-X (X: ferrite stabilizing element).

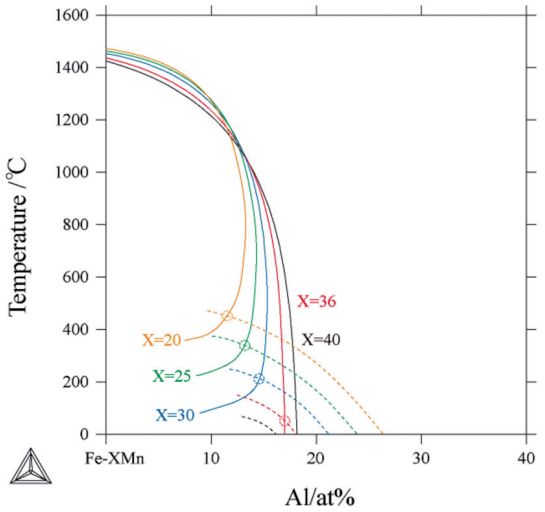

Fig. 7. $To^{\alpha/\gamma}$ lines in Fe-Mn-Al system.

4. HIGH STRENGTH Fe-Mn BASED ALLOYS WITH LOW DENSITY

Extensive work has been carried out for the Fe-Mn-Al-C and Fe-Mn-Si-C based alloys, which are the basic system for austenitic stainless steels without Ni and Cr[12–14], cryogenic

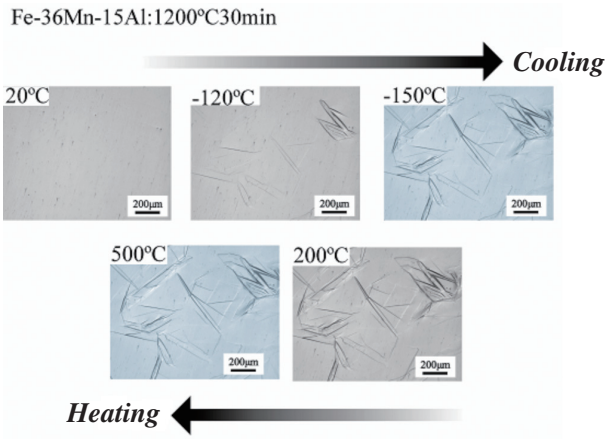

Fig. 8. Optical micrograph of martensite during heating and cooling in Fe-36Mn-15Al alloy.

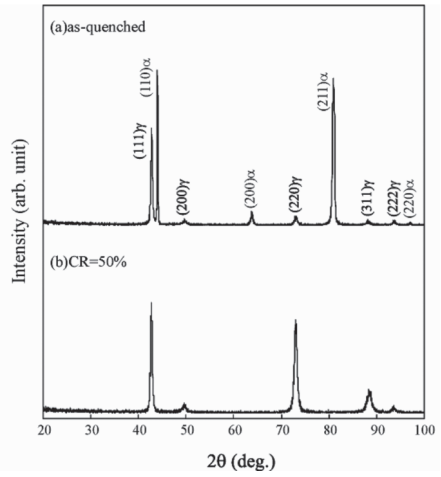

Fig. 9. XRD patterns taken from Fe-36Mn-15Al alloy sheets. (a) as-quenched and (b) cold-rolled to a reduction ratio of 50%.

materials[15–17] and magnetic alloys[18]. The mechanical properties of Fe-Mn-Al-C alloys show high strength and good ductility[19–22]. Since the Fe-Mn-C based alloys are very attractive for various applications, the thermodynamic database has been constructed by the CALPHAD approach[23], which is utilized for Fe, Al, Mn, Si, Cr and C. Thermodynamic assessments of binary and ternary systems, which had not been performed or need re-evaluation to extend them to multi-component systems, were carried out making use of previous and present experimental information. In the Fe-Al-C ternary system, κ-$Fe_3AlC_{1-\chi}$ ($E2_1$ perovskite carbide) is formed as shown in **Fig. 10** together with the isothermal section diagram at 1200°C[24]. The three sublattice model, $(Fe, Mn, Al)_3(Fe, Mn, Al)_1(C, Va)_1$, is applied to describe the non-stoichiometric composition, which is compared to the recent work of sublattice model, $(Fe, Mn)_3Al_1(C, Va)_1$[25]. The liquid, fcc (γ), bcc (α), cementite (M_3C), graphite (Gr) and other compounds (Al_8Mn_5, M_7C_3) are taken into account.

The calculated isothermal sections of Fe-20Mn-Al-C and Fe-30Mn-A1-C (mass %) at 1100°C are shown in **Fig. 11** compared with the experimental data[26]. Using the developed thermodynamic database, several alloys with low-density austenitic steels were designed. A typical example of stress-strain curves of Fe-20Mn-Al-C-5Cr alloys is presented in **Fig. 12**, which shows high strength (900–1200 MPa) and good ductility (20–65% elongation). **Figure 13** shows the stress-strain curves obtained in the Fe-20Mn-10Al-1.5C-5Cr γ alloy quenched in water and air cooled to room temperature from the annealing temperature of 1100°C, where the cooling rates of the water quenching and the air cooling were about 1100°C/s and about 15°C/s, respectively. The air-cooled specimen had a much higher yield strength than the water-quenched specimen and showed an upper yield point followed by almost constant flow stress. Such stress-strain behaviors are quite similar to that of the Fe-20Mn-11Al-1.8C-5Cr quinary γ alloy quenched in water, as shown in Fig. 12.

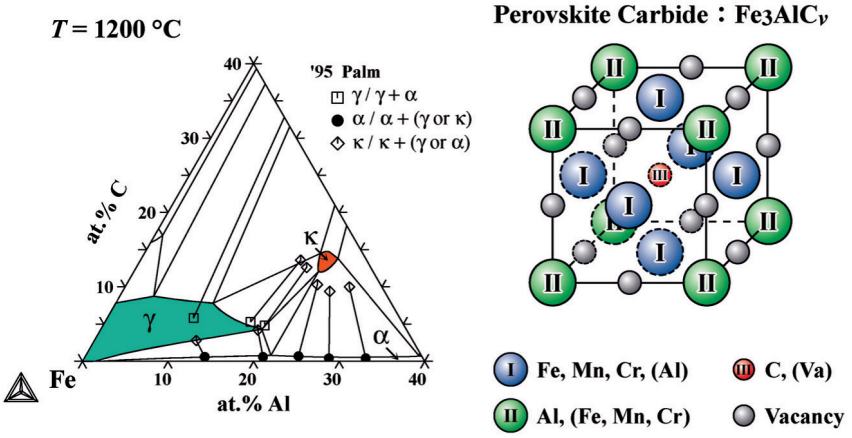

Fig. 10. Crystal structure of $E2_1$, perovskite carbide $Fe_3AlC_{1-\chi}$.

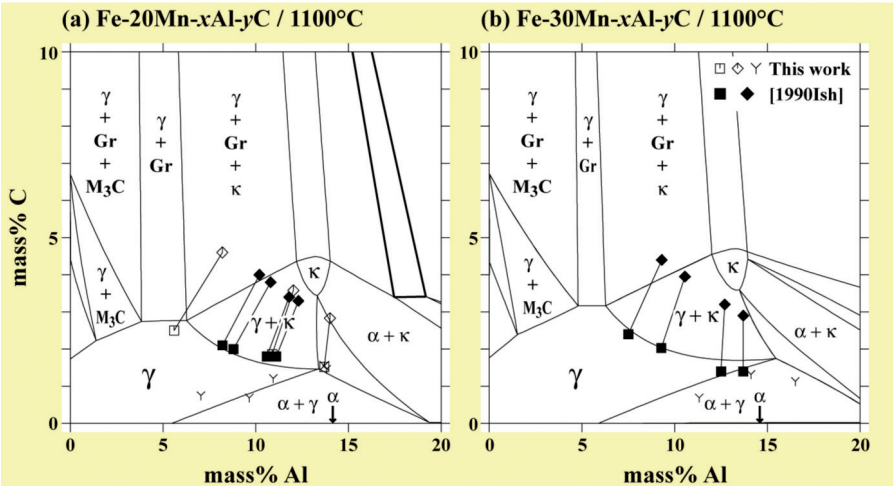

Fig. 11. Calculated isothermal section diagram compared with the observed ones at 1100°C. (a) Fe-20Mn-*x*Al-*y*C and (b) Fe-30Mn-*x*Al-*y*C.

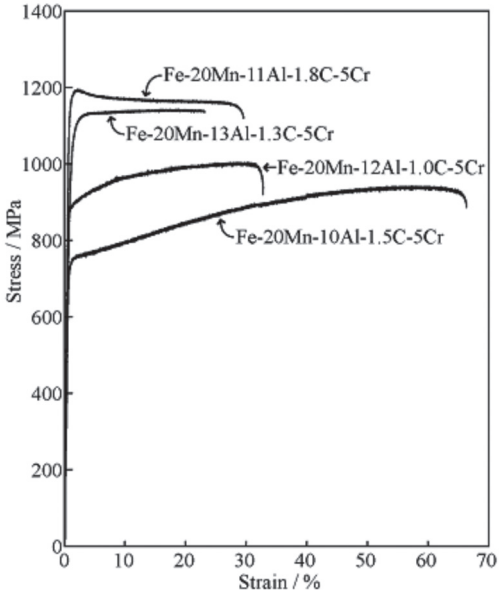

Fig. 12. Stress-strain curves at room temperature of Fe-Mn-Al-C-5Cr alloys.

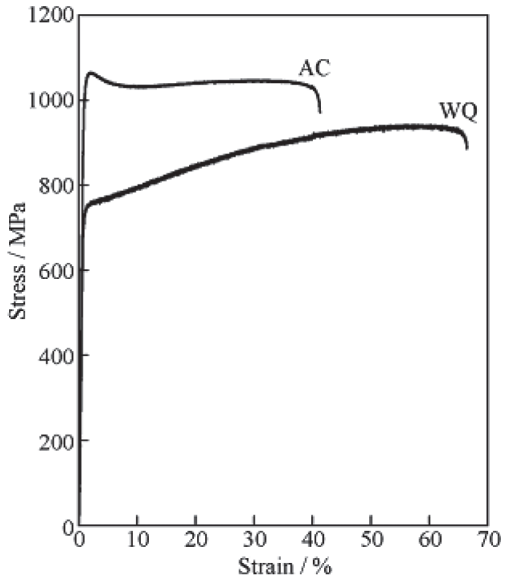

Fig. 13. Stress-strain curves in Fe-20Mn-10Al-1.5C-5Cr alloy annealed at 1100°C for 15 min followed by water quenching (WQ) and air cooling (AC) to room temperature.

Figures 14(a) and 14(b) show the diffraction pattern taken from the water-quenched and the air-cooled Fe-20Mn-10Al-1.5C-5Cr alloys, respectively. Although both patterns reveal extra spots between the fundamental reflections, which should indicate the formation of the κ phase with the perovskite structure, the intensity of the superlattice reflections in the air-cooled specimen is much higher than that in the water-quenched specimen. Figures 14(c) and 14(d) show dark field images of the $(100)_{\kappa}$ superlattice reflection in the water-quenched and air-cooled Fe-20Mn-10Al-1.5C-5Cr alloys, respectively. In the water-quenched specimen, very fine κ phase precipitates are slightly confirmed, while the cuboidal κ phase precipitates aligned in the $\langle 001 \rangle$ directions are clearly observed in the air-cooled specimen. The microstructure observed in the air-cooled Fe-20Mn-10Al-1.5C-5Cr alloy is very similar in morphology to that observed in Ni-based superalloys with the $\gamma + \gamma'$ two-phase. Therefore, it is concluded that high strength as well as a small work-hardening rate obtained in the Fe-Mn-Al-C(-Cr) alloys with a high C content are due to the nano-size precipitation of κ phase during cooling from the annealing temperature.

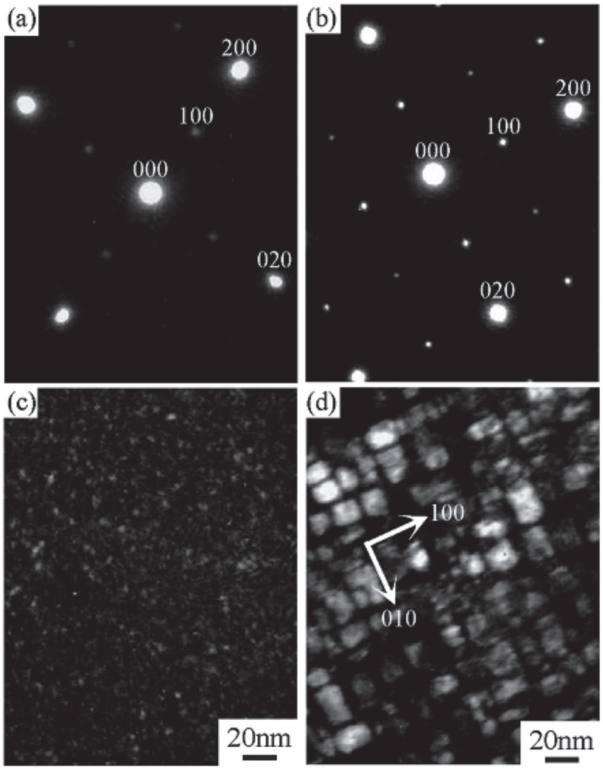

Fig. 14. Diffraction patterns taken from (a) water-quenched and (b) air-cooled Fe-20Mn-10Al-1.5C-5Cr alloy, and dark field images of the $(100)_{\kappa}$ superlattice reflection in (c) water-quenched and (d) air-cooled specimens.

Figure 15[27] shows the relationship between specific strength and tensile elongation in various steels, where the density of steels not previously reported was estimated. In all steels, a tendency for the tensile elongation to decrease with increasing specific strength can be observed. It is seen that the present Fe-Mn-Al-C(-Cr) alloys showed a higher specific strength than the conventional steels such as austenitic, ferritic, martensitic, precipitation hardened, dual-phase and super-toughness steels. Moreover, the specific strength of the present alloys is higher than that of Fe-Mn-Si-Al TWIP steels[28]. In addition, the present alloys also showed much higher yield strength than the TWIP steels. TRIP steels reported by Zackay *et al*,[29] possess a much higher specific strength

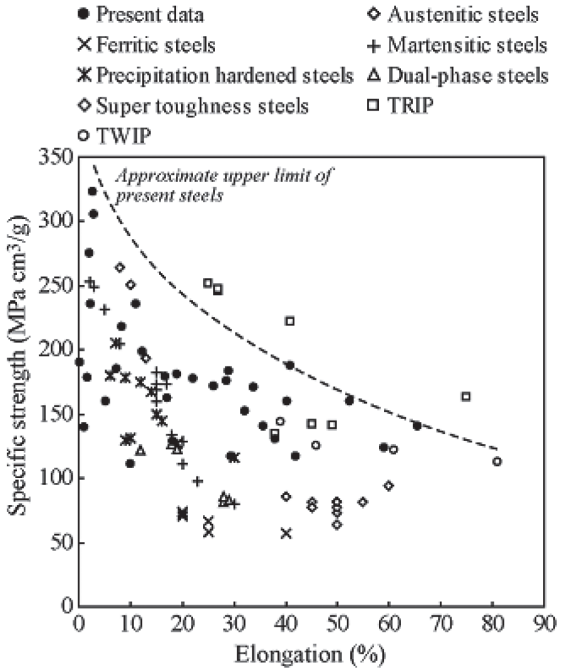

Fig. 15. Relationship between specific strength and tensile elongation in various steels.

than the present alloys. However, the high strength of the TRIP steels can only be obtained through a complicated thermo-mechanical process. On the other hand, the present alloys have an advantage in that both high specific strength and large tensile elongation can be obtained through simple processes controlling the annealing temperature and cooling rate.

5. STACKING FAULT ENERGY OF Fe-Mn BASED ALLOYS

Since stacking fault is related to many phenomena, e.g., mechanical properties, precipitation. martensitic transformation, corrosion resistance, etc., numerous studies have been conducted and the thermodynamic approach for estimating stacking fault energy has been developed[30–36]. A stacking fault in fcc can be regarded as a layer of cph phase, and therefore the Gibbs energy difference between the fcc and cph forms should be considered as substantial. Since the Gibbs energy of the cph phase is generally higher than that of the fcc phase, the parallel tangent construction is applied to estimate the fault concentration[35,37], that is, the Suzuki effect. The stacking fault energy (sfe) of Fe-Mn alloys by thermodynamic treatment has been studied[38–42] and is shown in **Fig. 16**, where Mn decreases sfe at a lower concentration of Mn but increases it with increasing Mn content. It is noted that the magnetic contribution to sfe is important[35,43,44] since the paramagnetic to anti-ferromagnetic transition occurs in the γ phase, which results in the increase of sfe at higher Mn concentration.

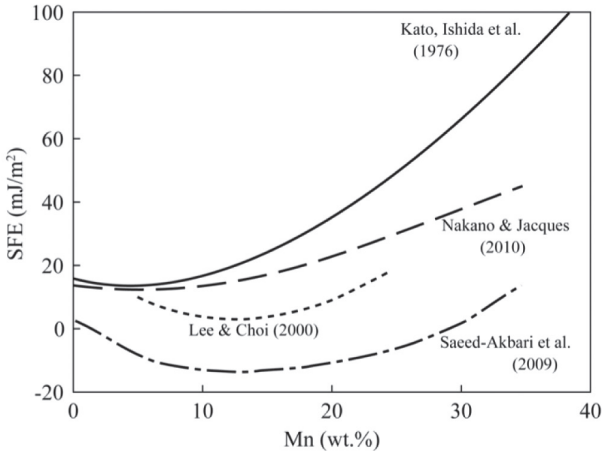

Fig. 16. Stacking fault energy of Fe-Mn system at room temperature.

In view of the effect of alloying elements on sfe, the $To^{\gamma/\varepsilon}$ temperature at which the Gibbs energy of γ and ε phases is equal is important. **Figure 17** shows the effect of alloying elements on $To^{\gamma/\varepsilon}$ temperature which was estimated by the *Ms* and *As* temperatures in the $\gamma \leftrightarrow \varepsilon$ martensitic transformation in Fe-17Mn (at %) alloy using the relation of $To\ (K) = (As + Ms)/2$[45]. This means that the alloying elements such as C, Ti, Nb, Cu, etc., which decreases $To^{\gamma/\varepsilon}$ temperature increases sfe, while the sfe is not so affected by the addition of Si, Co and Cr. **Figure18** shows the effect of alloying elements on the sfe of γ-iron[45] and the observed ones in the austenitic stainless steels[46]. It can be seen that there is a substantial agreement between the estimated and observed ones. It is noted that the alloying effect on sfe systematically changes in the periodic table. This is due to the similar tendency of the partial molar Gibbs energy difference $\Delta G_x^{\gamma/\varepsilon Fe}$ of alloying element between the γ and ε phases, which is expressed by the similar equations of (1) and (2)[45].

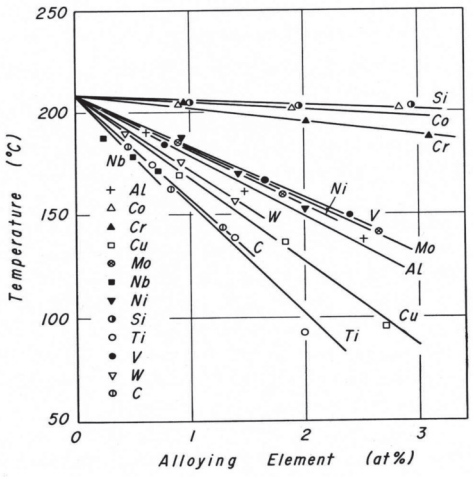

Fig. 17. Effect of alloying elements on $To^{\gamma/\varepsilon}$ temperature in Fe-17Mn alloy.

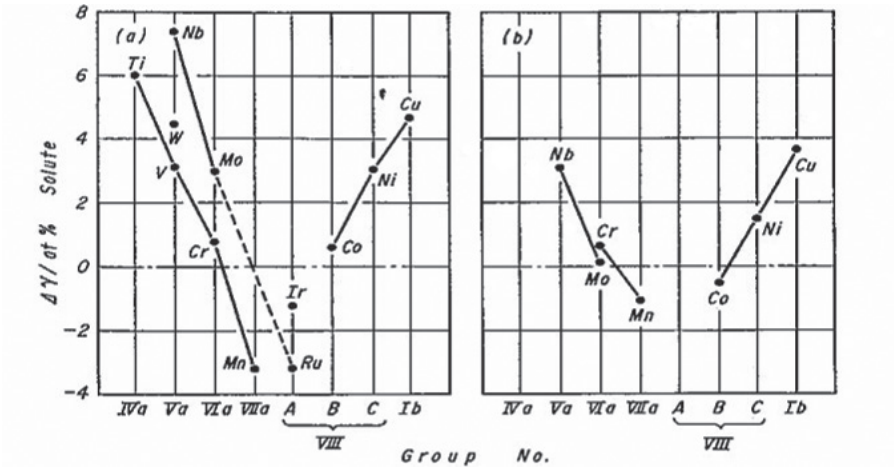

Fig. 18. Effect of alloying elements on the stacking fault energy of γ-iron.
(a) calculated and (b) observed.

6. SUMMARY

Phase equilibria between α (ferrite) and γ (austenite) in the Fe-Mn based alloys were briefly reviewed, focusing on the temperature dependence of the partial molar Gibbs energy change of Mn between α and γ phases and the peculiar shape of the γ-loop formed in the Fe-Mn-X (X: ferrite stabilizing element). The characteristic features of α/γ equilibria of Fe-Mn based alloys result in martensitic transformation from the ferrite to the austenite phase observed in the Fe-Mn-Al and Fe-Mn-Ga systems. The origin of this unique transformation and the magnetic properties of these systems accompanied by martensitic transformation were also shown. The thermodynamic database of the Fe-Mn based alloys, including the elements of C, Al, Si and Cr developed by the CALPHAD approach, was presented. The design of high-strength, low-density alloys using this database was presented.

ACKNOWLEDGMENT

The author would like to thank late Prof. Taiji Nishizawa for his interest and support. The author thanks Drs. R. Kainuma, I. Ohnuma, Y. Sutou, T. Omori and K. Ando for their help and useful discussions.

REFERENCES

1) A. Ledebur, Handbuch der Eisenhüttenkunde, Leibzig, **vol. 1** (1906) p.335.
2) C. Zener, *J. Metals,* **7** (1955) 619 .
3) C. Zener, *Trans. AIME,* **167** (1946) 513.
4) W. Oelsen and F. Wever, *Arch. Eisenhütt.,* **19** (1947/48) 97.
5) M. Hillert, T. Wada and H. Wada, *J. Iron Steel Inst.,* **205** (1967) 539.
6) K. Ishida and T. Nishizawa, *Trans. Jpn. Inst. Met.,* **15** (1974) 217.
7) K. Ishida, K. Shibuya and T. Nishizawa, *J. Jpn. Inst. Met.,* **37** (1973) 1305.
8) K. Ando, T. Omori, I. Ohnuma, R. Kainuma and K. Ishida, *Appl. Phys. Lett.,* **95** (2009) 212504.
9) T. Omori, K. Watanabe, R. Y. Umetsu, R. Kainuma and K. Ishida, *Appl. Phys. Lett.,* **95** (2009) 082508.
10) R. Umino, X. J. Liu, Y. Sutou, C. P. Wang, I. Ohnuma, R. Kainuma and K. Ishida, *J. Phase Equilibr. Diffusion,* **27** (2006) 54.
11) T. Omori, K. Ando, M. Okano, X. Xu, Y. Tanaka, I. Ohnuma, R. Kainuma and K. Ishida, *Science,* **333** (2011) 68.
12) S. K. Banerji, *Metal Prog.,* **113** (1978) 59.
13) R. Wang and F. H. Beck, *Metal Prog.,* **123** (1983) 72.
14) T. F. Liu, J. S. Chou and C. C. Wu, *Metall. Mater. Trans. A,* **21A** (1990) 1891.
15) J. Charles, A. Berghezan, A. Lutts and P. L. Pancoisne, *Metal Prog.,* **119** (1981) 71.
16) Y. G, Kim, J. K. Han and E. W. Lee, *Metall. Mater. Trans. A,* **17A** (1986) 2097.
17) J. E. Krzanowski, *Metall. Mater. Trans. A,* **19A** (1988) 1873.
18) I. Briggs, G. J. Russell and A. G. Clegg, *J. Mater. Sci.,* **20** (1985) 668.
19) T. Shun, C. M. Wan and J. G. Byrne, *Acta Metall. Mater.,* **40** (1992) 3407.
20) C. Y. Chao and C. H. Liu, *Mater. Trans.,* **43** (2002) 2635.
21) J. D. Yoo, S. H. Hwang and K. T. Park, *Metall. Mater. Trans. A,* **40A** (2009) 1520.
22) B. Bhattacharaya, A. S. Sharma, S. S. Hazra and R. K. Ray, *Metall. Mater. Trans. A,* **40A** (2009) 1190.
23) I. Ohnuma, T. Omori, Y. Sutou, R. Kainuma and K. Ishida, Presented at TOFA 2010, *Discussion Meeting on Thermodynamics of Alloys*, Porto (2010).
24) M. Palm and G. Inden, *Intermetallics,* **3** (1995) 443.
25) K-J. Chin, H-J. Lee, J-H. Kwak, J-Y. Kang and B-J. Lee, *J. Alloys & Compd.,* **505** (2010) 217.

26) K. Ishida, H. Ohtani, N. Satoh, R. Kainuma and T. Nishizawa, *ISIJ Int.,* **30** (1990) 680.
27) Y. Sutou, N. Kamiya, R. Umino, I. Ohnuma and K. Ishida, *ISIJ Int.,* **50** (2010) 893.
28) O. Grassel, L. Kruger, G. Frommeyer and L. W. Meyer, *Int. J. Plast.,* **16** (2000) 1391.
29) V. F. Zackay, E. R. Parker, D. Fahr and R. Bush, *Trans. Am. Soc. Met.,* **60** (1967) 252.
30) P. A. Flinn, *Acta Metall.,* **6** (1958) 631.
31) J. E. Dorn, *Acta Metall.,* **11** (1963) 218.
32) R. De Wit and R. E. Howard, *Acta Metall.,* **13** (1965) 655.
33) T. Ericsson, *Acta Metall.,* **14** (1966) 1073.
34) J. P. Hirth, *Metall. Trans.,* **1** (1970) 2367.
35) K. Ishida, *Phys. Stat. Sol. (a),* **36** (1976) 717.
36) G. B. Olson and M. Cohen, *Metall. Trans. A,* **7A** (1976) 1897.
37) M. Hillert, Lectures on the Theory of Phase Transformations, *AIME*, **1** (1975).
38) T, Kato, S. Fukui, M. Fujikura and K. Ishida, *Trans. ISIJ,* **16** (1976) 673.
39) Y-K. Lee and C-S Choi, *Metall. Mater. Trans. A,* **31A** (2000) 355.
40) A. Saeed-Akbari, J. Imlau, U. Prahl and W. Bleck, *Metall. Mater. Trans. A,* **40A** (2009) 3076.
41) J. Nakano and P. J. Jacques*, CALPHAD,* **34** (2010) 167.
42) C. Curtze and V.-T. Kuokkala, *Acta Mater.,* **58** (2010) 5129.
43) K. Ishida, *Phil. Mag.,* **32** (1975) 663.
44) A. P. Miodownik*, CALPHAD,* **4** (1978), 143.
45) K. Ishida and T. Nishizawa, *Trans. Jpn. Inst. Met.,* **15** (1974) 225.
46) D. Dulieu and J. Nutting, *Metallurgical Developments in High-alloy Steels*, The Iron and Steel Institute of London, Special Report, **No. 86** (1964) 140.